



Effective Removal of Molybdenum(VI) from Aqueous Solution Using Polyethylene Polyamine-Grafted Sugarcane Bagasse Biosorbent

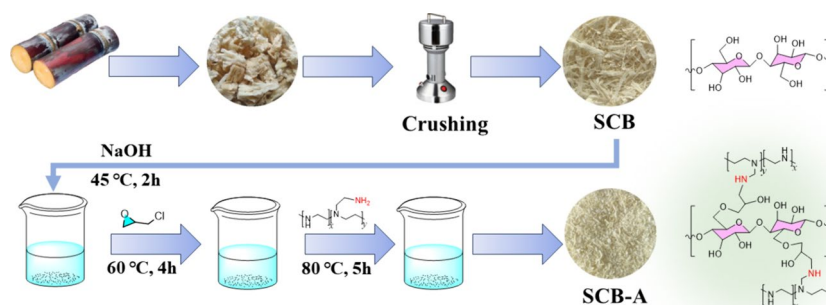
Miaomiao Peng¹ · Chen Xi¹ · Keyu Shen¹ · Yangjing Tan¹ · Fei Li^{1,2,3}

Received: 25 November 2023 / Accepted: 14 May 2024 / Published online: 3 June 2024
© The Minerals, Metals & Materials Society 2024

Abstract

A novel greenness and low-cost biosorbent was prepared by polyethylene polyamine-modified waste biomass of sugarcane bagasse in this study, which was used to remove molybdenum(VI) from aqueous solution. The structural properties and adsorption mechanism of this amine-functionalized sugarcane bagasse adsorbent (SCB-A) on Mo(VI) were investigated by SEM–EDS, BET, TG, FTIR, XPS, and batch adsorption experiments. The results show that the adsorption reaction between SCB-A and Mo(VI) was a spontaneous endothermic process, and its theoretical maximum adsorption capacity was about 231.48 mg/g. The adsorption capacity was 8.93-fold compared to that of pristine sugarcane bagasse. This adsorption process was more consistent with the Langmuir model and pseudo-second-order kinetics model, indicating that this process was monolayer adsorption on a homogeneous surface and the adsorption rate was controlled by the chemisorption process. SCB-A possessed great reusability, maintaining a stable adsorption capacity after five recycles. For the adsorption toward Mo(VI), SCB-A also exhibited superior selectivity in a multi-ion coexistence solution. Therefore, SCB-A has tremendous potential in the economically and feasible removal of Mo(VI) from wastewater.

Graphical Abstract



Keywords Sugarcane bagasse · Polyethylene polyamine · Molybdenum · Adsorption

The contributing editor for this article was Grace Ofori-Sarpong.

Miaomiao Peng and Chen Xi have equally contributed to this manuscript.

✉ Fei Li
lifei__123456789@163.com

¹ School of Chemistry and Chemical Engineering, Jishou University, Jishou 416000, Hunan, China

² Key Laboratory of Mineral Cleaner Production and Exploit of Green Functional Materials in Hunan Province, Jishou 416000, Hunan, China

³ The Collaborative Innovation Center of Manganese-Zinc-Vanadium Industrial Technology (The 2011 Plan of Hunan Province), Jishou 416000, Hunan, China

Introduction

Molybdenum, a rare and valuable metal with a high melting point, good conductivity and wear resistance, and low thermal expansion coefficient, has been widely applied in crucial areas such as alloys, catalysts, and medicine [1, 2]. The recovery of molybdenum from various sources and the reduction of environmental problems aroused more and more attention from metallurgists with the increasing demand continuously for molybdenum globally. Although molybdenum is a necessary microelement for plants and animals, it can cause environmental problems and many diseases such as anemia, delayed growth, and even death with high concentrations of molybdenum [1, 3]. Molybdenum forms ions in different oxidation states, and the oxyanion MoO_4^{2-} (Mo(VI)) is the main form of soluble molybdenum in environmental pollution [1]. The allowable concentration of molybdenum(VI) in potable water should be below 0.07 mg/L [4]. Thus, the selective recognition and removal of molybdenum(VI) from aqueous solution is essential.

Several methods, such as solvent extraction [5], ion exchange [6], chemical precipitation [7], and adsorption [8], have been used for removing metal ions from aqueous solution. Solvent extraction has the advantage of excellent selective recognition, high extraction capacity, and simple operation. However, the organic phase used in solvent extraction is usually toxic, flammable, and detrimental to the environment. The advantage of ion exchange is good reusable, excellent removal capacity, and simple device, but it has some drawbacks such as poor selectivity and a large amount of wastewater. The merits of chemical precipitation are low cost and simple process, but it possesses the possibility of secondary pollution. Adsorption is an economical and effective method to recover trace molybdenum from aqueous solution due to its high efficiency, simple operation, and no secondary pollution. Thus, adsorption is applied for the selective recognition and removal of molybdenum(VI) from aqueous solution in this study to reach the purpose of high efficiency, greenness, and sustainability. Various adsorption materials have been used for removing metal ions, including activated carbon, silica gel particles, and alumina. However, some drawbacks, such as expensive cost, long adsorption time, low selectivity, and poor recyclability, must be considered in these adsorbents from actual applications. Thus, it is significant to synthesize adsorbents with low cost, selectivity recognition, recyclability, high adsorption capacity, and rapid adsorption–desorption to remove molybdenum(VI) from aqueous solution.

Biosorbents as efficient and economical have obtained more and more attention for removing heavy metals in

wastewater, especially low-cost agricultural waste such as sugarcane bagasse [9–11]. The sugarcane bagasse consists of 50% cellulose, 27% polyose, and 23% lignin and is one of the best waste materials of lignocellulosic with low cost and large quantities [10, 12]. In the previous report, the surface modification by amine groups could modify the adsorbent property and enhance its adsorption capacity for metal ions due to the specific surface charge of amine groups [10, 11]. For instance, the adsorption capacities of ethyl cellulose film increased by hyperbranched polyethylenimine-functionalized [13]. Although multiple researches on lignocellulosic waste modification have been published around the world in this field, sugarcane bagasse modification for removing molybdenum(VI) has rarely been conducted, and no studies on extending polyethylene polyamine-grafted sugarcane bagasse to remove molybdenum(VI) have not been reported.

Herein, an amine-functionalized sugarcane bagasse adsorbent (SCB-A) was synthesized by using polyethylene polyamine to reach selectivity recognition and removal of molybdenum(VI) from aqueous solution in this work. Polyethylene polyamine was immobilized on sugarcane bagasse substrates to explore the adsorption property of the polyethylene polyamine structures on molybdenum(VI). The superiority of synthesized SCB-A for molybdenum(VI) adsorption was proved by adsorption isotherm, regeneration, and competitive adsorption experiments. Furthermore, the structural properties and possible adsorption mechanism of SCB-A for molybdenum(VI) were analyzed by using different characterizations and batch adsorption experiments under different conditions. This work aims to supply useful references to develop a more economical and feasible material for the removal of Mo(VI) from wastewater.

Experimental

Materials

The sugarcane bagasse used in this work was collected from the Guangxi Sugarcane Mill. Polyethylene polyamine ($\text{C}_{2n}\text{H}_{5n}\text{N}_n$, CAS: 68131-73-7) was supplied by Aladdin. Ammonium molybdate (CAS: 12054-85-2) was afforded from the Tianjin Chemical Plant. Nitric acid (HNO_3 , CAS: 7697-37-2) and sodium hydroxide (NaOH, CAS: 1310-73-2) were purchased from Shanghai Chemical Company. 95% ethanol (CAS: 64-17-5), 50% Mangan nitrate water solution (CAS: 10377-66-9), and cadmium nitrate (CAS: 10325-94-7) were provided by Tianjin Kemiou Chemical Reagent Co., Ltd. Copper(II) nitrate trihydrate (CAS: 10031-43-3) and nickel(II) nitrate hexahydrate (CAS: 13478-00-7) were provided by Xilong Scientific. De-ionized water was used

in each experiment. All reagents used in this work were of analytical grade.

Preparation of SCB-A

Amine-functionalized sugarcane bagasse adsorbent (SCB-A) was synthesized by the sugarcane bagasse and polyethylene polyamine. Firstly, the waste sugarcane bagasse was used as the raw material to prepare the sugarcane bagasse substrates (SCB) as follows: The waste sugarcane bagasse was washed sequentially with de-ionized water and ethanol solution until the sugars were removed. After washing, sugarcane bagasse was dried in a hot air oven at 60 °C for two days. Then, the drying sugarcane bagasse after crushing was marked as SCB.

The synthesis protocol for the synthesis of SCB-A from SCB is displayed in Fig. 1. Briefly, 5 g SCB was dissolved in 300 ml 1 mol/L NaOH solution and agitated for 2 h at 45 °C in a water bath pot at 150 rpm, and then filtered. Secondly, grafting was achieved by adding 20 mL epichlorohydrin and 100 ml ethanol solution, followed by stirring for 4 h at 60 °C. The sugarcane bagasse of grafting epichlorohydrin was washed twice with ethanol solution by stirring for 10 min each at 40 °C. Next, 20 mL polyethylene polyamine and 100 ml ethanol solution were added by stirring for 5 h at 80 °C, and then filtered. Finally, the resulting amine-functionalized sugarcane bagasse (SCB-A) was washed sequentially with the ethanol solution at 40 °C for each 20 min and de-ionized water until the pH of the washings reached neutrality, and then dried in a hot air oven at 60 °C for 2 days.

Instruments

The concentrations of metal ions in solution were determined using Inductively coupled plasma atomic emission

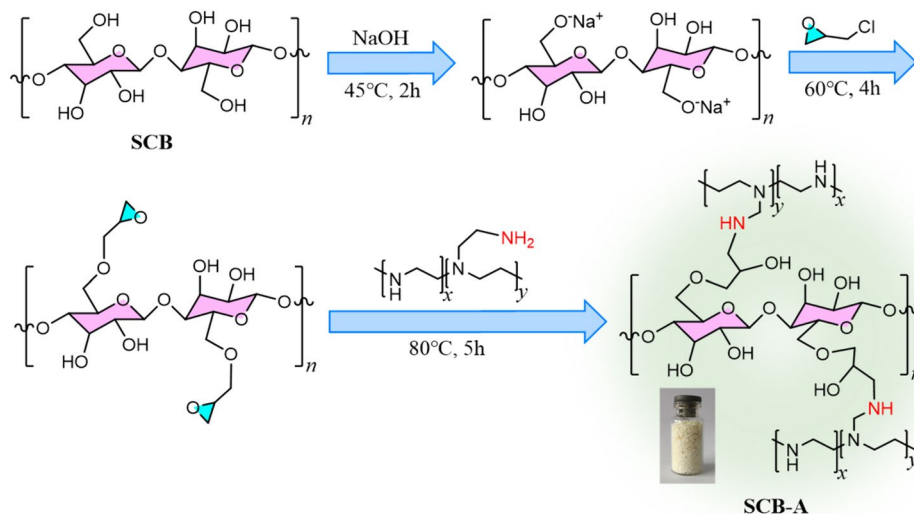
spectrometry (ICP-OES) (Avio200, PerkinElmer, American). The samples were characterized by using Scanning electron microscopy (SEM, Tescan Mira Lms, Czech Republic) and energy-dispersive spectroscopy (EDS), Thermo-gravimetric analyzer (TGA 2, Mettler Toledo, Switzerland), Automatic Specific Surface and Porosity Analyzer (BET, Micromeritics ASAP 2460, American), Fourier transform infrared spectroscopy (FTIR, Nicolet iS10, ThermoFisher, American), and X-ray photoelectron spectroscopy (XPS, Thermo Scientific K-Alpha, American).

Adsorption Experiments

Mo(VI) solution at different concentrations was prepared by ammonium molybdate. The Mo(VI) solution and quantitative adsorbent (SCB-A) were mixed in conical flasks and thus placed in a constant temperature water bath shaker under different conditions for batch adsorption experiments. The separation of solution and adsorbent after adsorption (SCB-A-Mo(VI)) was used by the funnel. The concentration of Mo(VI) in the solution was determined by using ICP-OES.

In the preliminary experiments, the effects of different initial pH values (from 1 to 6) and adsorbent dosages (from 0.5 to 2.5 g/L) on the Mo(VI) adsorption were evaluated under corresponding conditions. The adsorption kinetics experiments were carried out in the range of 5–300 min at pH = 2 and 298 K. The equilibrium adsorption isotherms of Mo(VI) at 298 K, 308 K, and 318 K of temperature and initial concentration range of 100–500 mg/L were investigated with pH 2. The competitive experiment was carried out using a multi-ion coexistence solution (Cd, Cu, Mn, Ni, and Mo) at 298 K for 3 h to evaluate the selective performance of SCB-A for Mo(VI). The regeneration experiment was performed by different eluents (NaOH, EDTA, and

Fig. 1 Schematic diagram for the preparation of SCB-A from SCB



HNO₃) at 298 K for 3 h to evaluate the regeneration ability of SCB-A. The SCB-A was washed to neutral with distilled water before each adsorption cycle.

The adsorption capacity (q_e) and adsorption efficiency (E) of SCB-A were calculated as Eqs. (1) and (2), respectively [14].

$$q_e = \frac{(C_0 - C_e) \times V}{m}, \quad (1)$$

$$E = \frac{(C_0 - C_e)}{C_0} \times 100\%, \quad (2)$$

where q_e is the adsorption capacity (mg/g); C_0 is the initial concentrations of metal ions (mg/L); C_e is the equilibrium concentrations of metal ions (mg/L); V is the volume of solution (mL); m is the adsorbent weight (mg); E is the adsorption efficiency (%).

The selective performance for target metal ions was evaluated by the distribution coefficient (K_d) and selectivity coefficient (K), which are calculated as Eqs. (3) and (4) [14, 15].

$$K_d = \frac{q_e}{C_e}, \quad (3)$$

$$K = \frac{K_d - \text{Mo(VI)}}{K_d - X}, \quad (4)$$

where q_e represents the adsorption capacity (mg/g); C_e is the equilibrium concentration of metal ions (mg/L); K_d is the distribution coefficient; K is the selectivity coefficient; X is the Cd, Cu, Mn, and Ni.

Results and Discussion

Characterization

SEM-EDS Analysis

The SEM-EDS analysis was carried out to study the surface morphology and compositional distribution of SCB, SCB-A, and SCB-A-Mo(VI). As presented in Fig. 2a1 and a2, the surface of SCB exhibited a smooth cellulose structure. The surface of SCB-A was observed as a wrinkle-like microstructure, as shown in Fig. 2b1 and b2, indicating the successful modification. The rough cellulose structure was found in the SEM of SCB-A-Mo(VI) as shown in Fig. 2c1 and c2, which is possibly caused by the successful adsorption of Mo(VI) with SCB.

To further prove whether polyethylene polyamine was successfully grafted onto sugarcane bagasse, EDS was used to conduct the elemental quantitative analysis. As shown

in Fig. 2a4 and b4, the contents (wt%) of N in SCB and SCB-A were 0.00 and 0.67%, respectively. In contrast, the nitrogen content of SCB-A is higher than that of SCB, indicating the successful grafting of polyethylene polyamine onto sugarcane bagasse [15]. As shown in Fig. 2c3, Mo(VI) (wt% 34.26%) was distributed on the surface of SCB-A uniformly, demonstrating the successful adsorption of Mo(VI) with SCB-A.

BET and Thermogravimetry Analysis

The BET isotherms and physical parameters such as BET surface area and pore volume of SCB and SCB-A were studied, as shown in Fig. 3a and b and Table 1. Results show that the pore volume BET and surface area of SCB-A were 0.0045 cm³/g and 1.8102 m²/g, respectively. SCB-A had a lower pore volume (0.0045 cm³/g) compared to SCB (0.0050 cm³/g). The possible cause is owing to the production of smaller pores in SCB-A after the graft of polyethylene polyamine. The BET surface area of SCB-A (1.8102 m²/g) was found to be smaller than that of SCB with the value of 1.9341 m²/g. BET surface area and pore volume of SCB-A decrease compared to SCB, demonstrating the success of polyethylene polyamine-grafted on sugarcane bagasse [8, 13].

The thermostability of adsorbent before (SCB-A) and after adsorption (SCB-A-Mo(VI)) was investigated by thermogravimetric (TG) and their differentials (DTG) analysis. The experiments were carried out by temperature range from 30 to 800 °C with a heating rate of 20 °C/min. Figure 3c shows the relationship between the mass loss of SCB-A and temperature, indicating the decomposition of SCB-A can be divided into three stages. In the first stage, 10% of the mass loss at the temperature from 50 to 170 °C, arising from the evaporation of moisture. The mass loss in the second stage occurs at the temperature range from 170 to 410 °C is about 75%, which corresponds to the decomposition of organic molecules in SCB-A. In the last stage, the final mass loss above 410 °C was due to charring [16, 17]. Besides, the overall mass loss of SCB-A-Mo(VI) was 32.2% up to 800 °C, higher than that of SCB-A (8.2%). The result demonstrates the good thermal stability of SCB-A and its successful adsorption of Mo(VI) [18].

Batch Adsorption Experiments

Effect of Initial pH Value

The pH value of the solution is one of the most critical factors in the absorption process that affects both the distribution of molybdenum ion species and the surface performance of the adsorbent [14, 19]. To explore the influence of pH on the adsorption behavior of SCB-A for

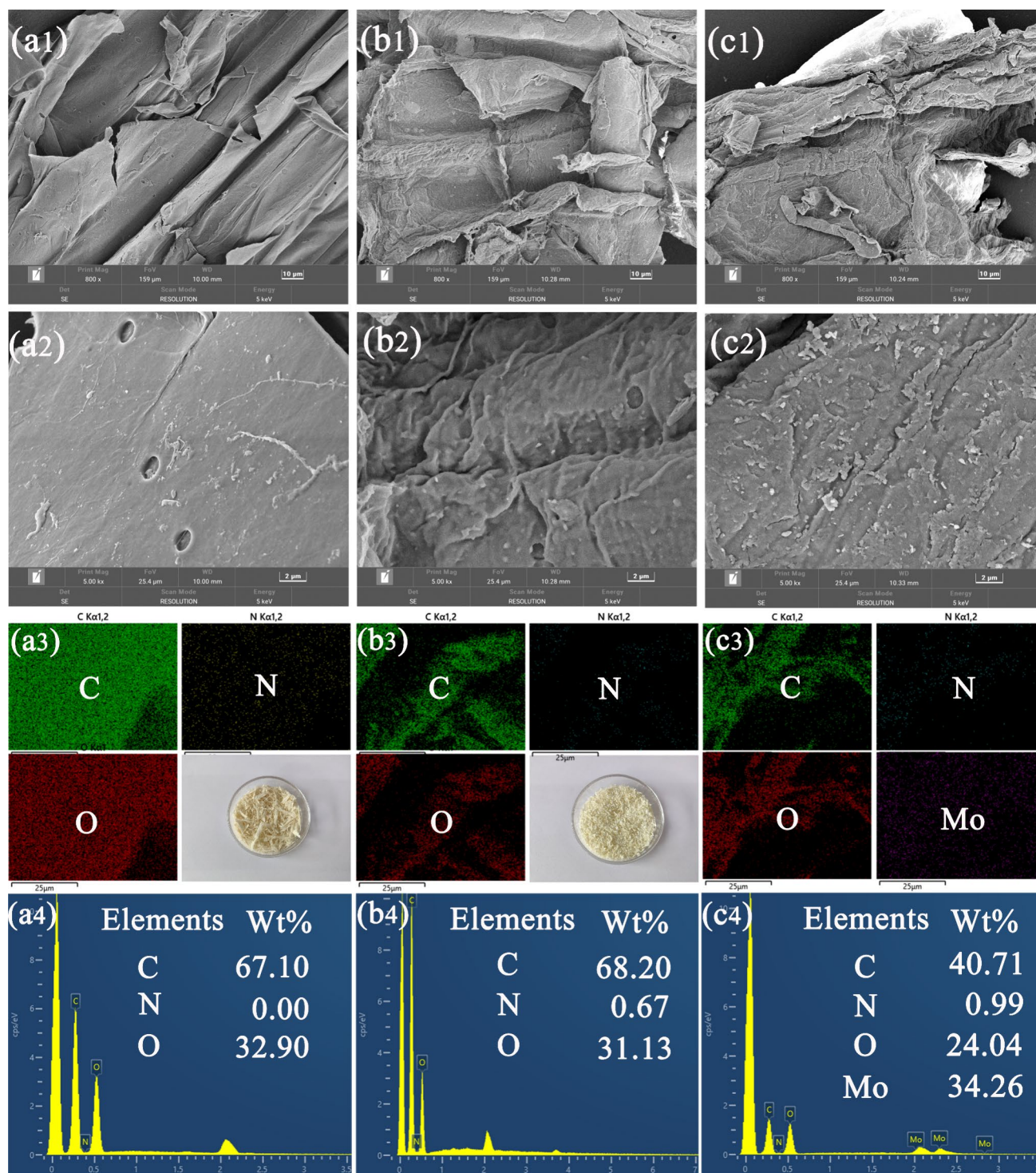


Fig. 2 SEM-EDS a: SCB, b: SCB-A, c: SCB-A-Mo(VI)

molybdenum(VI), the adsorption experiment was carried out under different pH values (from 1 to 6), with results shown in Fig. 4a. It was observed that the adsorption capacity of SCB-A exhibited a trend of increasing first and then decreasing as pH increases. For an initial

molybdenum(VI) concentration of 300 mg/L, the adsorption capacity (q_e) increased from 18.9 to 208.1 mg/g, as the pH value increased from 1.0 to 2.0, respectively. Beyond this point, a decrease was noted between pH 2.0

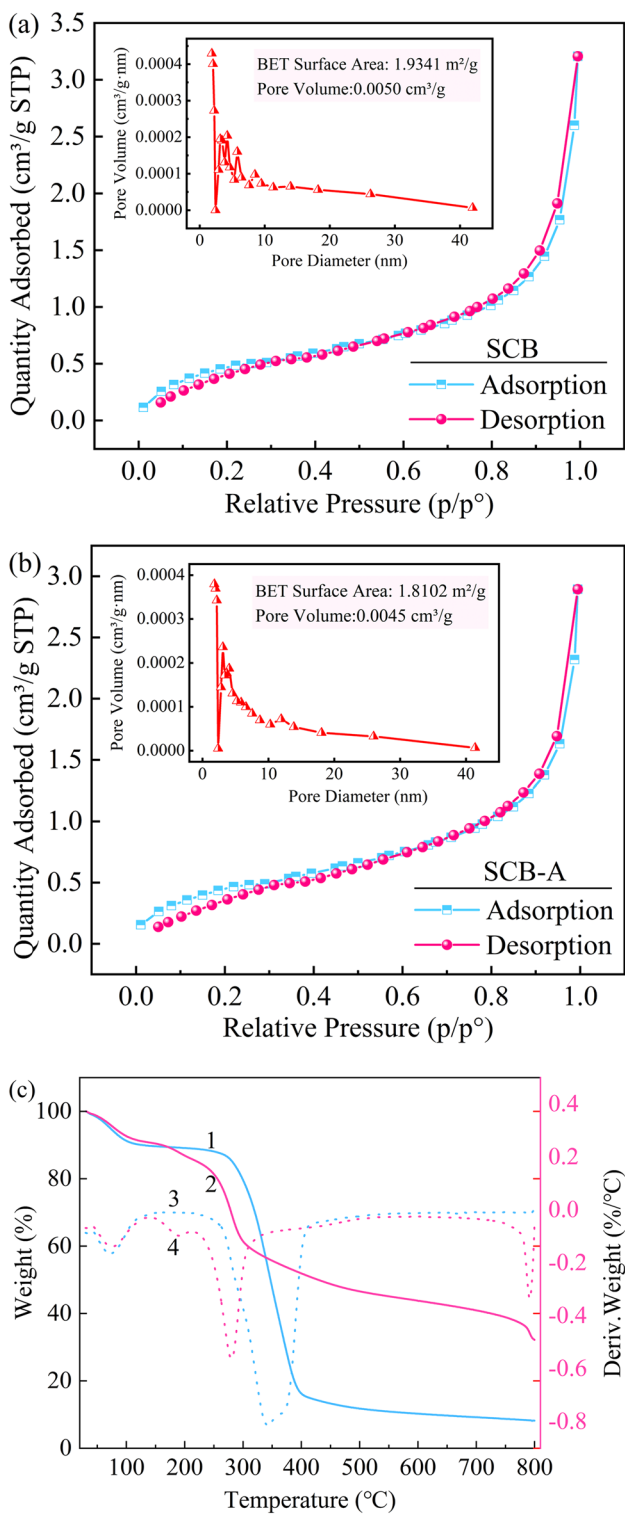


Fig. 3 BET isotherms of **a** SCB and **b** SCB-A; **c** TG and DTG curves of SCB-A before (1, 3) and after (2, 4) adsorption

Table 1 The physical parameters of SCB and SCB-A

Type	BET surface area (m ² /g)	Total pore volume (cm ³ /g)	Average pore diameter (nm)
SCB	1.9341	0.0050	10.2580
SCB-A	1.8102	0.0045	9.8923

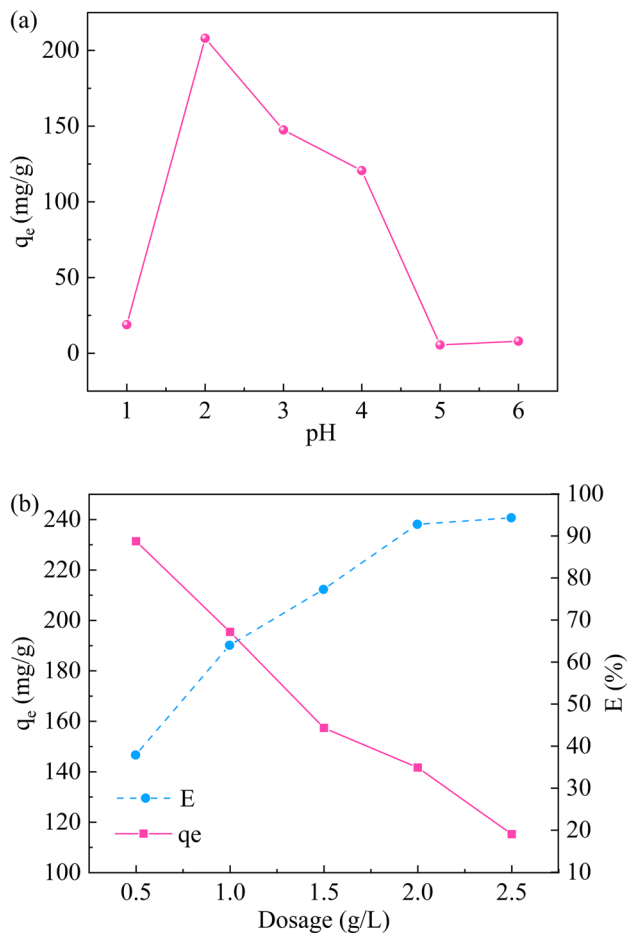


Fig. 4 Effect of initial pH value (**a**: [Mo]=300 mg/L, *t*=5 h, *T*=25 °C) and adsorbent dosage (**b**: pH=2, [Mo]=300 mg/L, *t*=5 h, *T*=25 °C) on the adsorption capacity of SCB-A for Mo(VI)

and 5.0. Obviously, at a lower pH value (pH 2), the maximum adsorption capacity of SCB-A was achieved.

A possible explanation is the different potential states of groups on the adsorbent surface, species of molybdenum ions in solution and ability of competitive adsorption between -OH in aqueous solution and molybdenum anion with the change of pH value. At low pH, the amine groups (-NH₂) of SCB-A were protonated to form -NH₃⁺ groups, which would endow the adsorbent with more positive charges [20]. Moreover, the principal forms of molybdenum(VI) cationic MoO₂⁺ are converse to anion H₃Mo₇O₂₄³⁻ and then to various

anions with pH from 1.0 to 2.0 and then increase, respectively [21]. The molybdenum(VI) anions could be absorbed by positive charges of the adsorbent SCB-A surface via electrostatic absorption. With the number of molybdenum(VI) anions increased with the pH value from 1.0 to 2.0, the ability of electrostatic absorption between the SCB-A and molybdenum(VI) increased, causing an increase in the adsorption capacity of the adsorbent. However, after the pH value exceeded 2, the poor adsorption capacity was probably caused by the decreased number of protonated $-\text{NH}_3^+$ groups on SCB-A to reduce the ability of electrostatic absorption and the competition absorption between $-\text{OH}$ in aqueous solution and molybdenum(VI) anions with SCB-A. Therefore, the optimal pH in the molybdenum(VI) adsorption of SCB-A is 2, which was suited for subsequent studies.

Effect of Adsorbent Dosage

The adsorption performance was also influenced by the adsorbent dosage, which was correlated with the economics. The influence of adsorbent dosage (from 0.5 to 2.5 g/L) on the adsorption capacity of molybdenum(VI) was studied, and the results are shown in Fig. 4b. The adsorption capacity decreased from 231.4 to 115.2 mg/g and the removal efficiency increased with increasing adsorbent dosage from 0.5 to 2.5 g/L. A higher dosage increased the total number of available adsorption sites, thus improving the removal efficiency. The reason is that the unsaturated sites increased with increasing adsorbent dosage, causing a reduction in the adsorption capacity of adsorbent per unit weight [22]. However, superfluous dosage may cause a reduction in adsorption capacity and an increase in resource consumption. Therefore, in synthetically considering, 1 g/L of the adsorbent dosage was selected for further experiments.

Adsorption Kinetics

Adsorption kinetic depicts the solute uptake rate governing the contact time of the sorption reaction. It is a process of the adhesion and accumulation of metal ions to the adsorbent surface and one of the significant characteristics that define the sorption efficiency [14, 19]. The kinetics of molybdenum(VI) adsorption by SCB and SCB-A were investigated in the range of 5–300 min, and results are presented in Fig. 5 and Table 2. Results show that the adsorption capacity of SCB-A was significantly higher than that of SCB (about 8.93 times), indicating the polyethylene polyamine-grafted success and the adsorption capacity of sugarcane bagasse after modification was significantly improved. The adsorption capacity of SCB-A is rapidly increased with increasing time, and then the adsorption capacity increases slowly and tends to equilibrium. The removal of molybdenum(VI) is highly rapid in the beginning adsorption

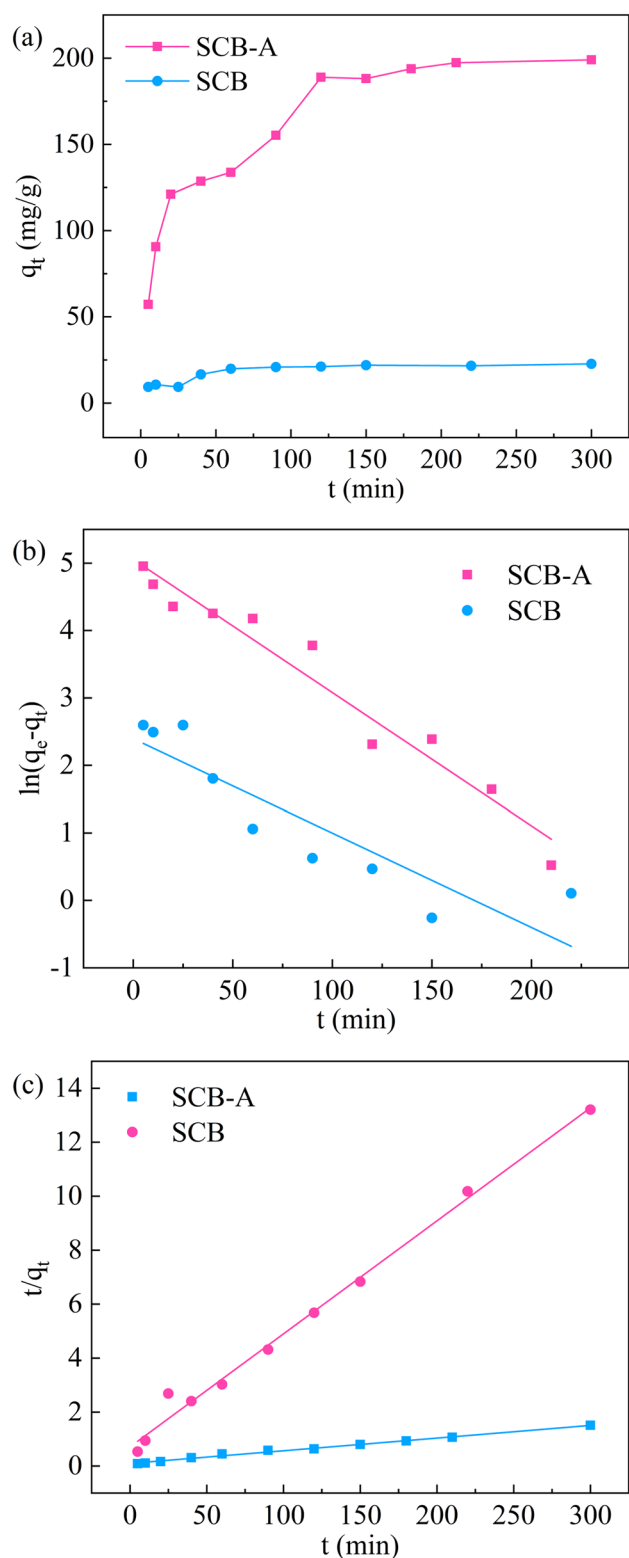


Fig. 5 a Effect of time on the adsorption capacity on Mo(VI); b Fitting data with the pseudo-first-order kinetic model; c Fitting data with the pseudo-second-order kinetic model; (pH=2, [Mo]=300 mg/L, $t=5$ h, $T=25$ °C)

Table 2 Kinetics parameters of Mo(VI) adsorption

	C_i (mg/L)	pseudo-first-order			pseudo-second-order		
		k_1 (min ⁻¹)	q_e (mg/g)	R^2	k_2 (g/mg·min)	q_e (mg/g)	R^2
SCB	300	1.40E-02	10.97	0.809	2.47E-03	23.88	0.999
SCB-A	300	1.98E-02	156.83	0.957	2.25E-04	213.22	0.971

process because of a large number of active sites and small mass transfer resistance on the surface of SCB-A. However, fewer active sites could be available and the adsorption rate reduced as the coverage of SCB-A by molybdenum(VI) ion increases, until reaching an equilibrium status [8].

To elucidate the controlling mechanisms in the adsorption process, the kinetic data were analyzed using two kinetics models, such as the pseudo-first-order (Eq. 5) and pseudo-second-order kinetics (Eq. 6) [23]. The determination coefficient (R^2) and kinetic parameters of two kinetic equations are summarized in Table 2. The pseudo-second-order of SCB-A (the correlation coefficients $R^2=0.971$) exhibited a relatively better consistency with the sorption data than the pseudo-first-order ($R^2=0.957$). Besides, the adsorption capacity value calculated through the pseudo-second-order kinetics model is approximately the same as the experimental value. These often demonstrate that the adsorption process of SCB-A for molybdenum(VI) can be more properly described by the pseudo-second-order kinetics model, indicating that the adsorption rate was mainly controlled by the chemisorption process, and a chemical or electrostatic attraction between the adsorbent and the adsorbate possibly [24–26].

$$\ln(q_e - q_t) = \ln q_e - k_1 t, \quad (5)$$

$$\frac{t}{q_t} = \frac{1}{k_2 q_e^2} + \frac{t}{q_e}, \quad (6)$$

where t is contact time (min); q_t is adsorption capacity at time t (mg/g); q_e is the adsorption capacity at equilibrium (mg/g); k_1 is the rate constant of pseudo-first-order adsorption (min⁻¹); k_2 is the rate constant of pseudo-second-order adsorption (g/(mg·min)).

Adsorption Isotherms and Thermodynamics

Adsorption isotherm could be applied to elucidate the adsorption characteristics of molybdenum(VI) onto the SCB-A, i.e., the interactions between molybdenum(VI) and sorption sites, and the maximum adsorption capacity [14]. For this purpose, the adsorption isotherms of molybdenum(VI) by the SCB-A were investigated in various initial concentrations of molybdenum(VI) (100–500 mg/L) at different temperatures (298 K, 308 K and 318 K), as shown in Fig. 6

and Table 3. Results show that the adsorption capacity of SCB-A for Mo(VI) increased with the increasing initial content of molybdenum(VI) in the solution. The possible reason is that SCB-A has more unsaturated adsorption sites under low initial content of molybdenum(VI), and then the adsorption capacity of SCB-A for Mo(VI) gradually increases and reaches equilibrium with the initial content of molybdenum(VI) increasing.

The experimental data were analyzed using Langmuir and Freundlich isotherm models, as shown in Fig. 6b and c. The Langmuir equilibrium model supposes that monolayer adsorbate is adsorbed on the surface of the adsorbent when saturated, and each active site is equivalent. The Freundlich model predicts that infinite adsorption will happen, and allows the second layer of the adsorbate to form before monolayer adsorbate is filled, and thus the adsorbate concentration adsorbed by the adsorbent rises exponentially with increasing the adsorbate concentration [27]. The nonlinear forms of the Langmuir and Freundlich are given in Eqs. (7) and (8), respectively [14, 23]. As presented in Fig. 6b and c, the result of the Langmuir model was fitted better than the Freundlich model, and the obtained isothermal adsorption parameters are listed in Table 3. The high R^2 values further indicated that molybdenum(VI) adsorption on SCB-A was consistent with the Langmuir model, indicating that molybdenum(VI) adsorption by SCB-A was monolayer adsorption on the homogeneous surface [28].

$$\frac{C_e}{q_e} = \frac{C_e}{q_m} + \frac{1}{q_m K_L}, \quad (7)$$

$$\ln q_e = \ln K_F + \frac{1}{n} \ln C_e, \quad (8)$$

where q_e is the equilibrium adsorption capacity (mg/g); C_e is the equilibrium concentration (mg/L); q_m is the theoretical maximum adsorption capacity (mg/g); K_L is Langmuir constant (L/mg); K_F and $1/n$ are Freundlich constants (L^{1/n} · mg^{1-1/n}/g).

The thermodynamics parameters of adsorption were usually used to elucidate the adsorption behavior, including the standard Gibbs free energy change (ΔG^0 , kJ/mol), enthalpy change (ΔH^0 , kJ/mol), and entropy change (ΔS^0 , J/mol·K) (Table 4), as expressed in Eqs. (10) and (11), respectively. With this purpose, the adsorption experiments were carried out using the

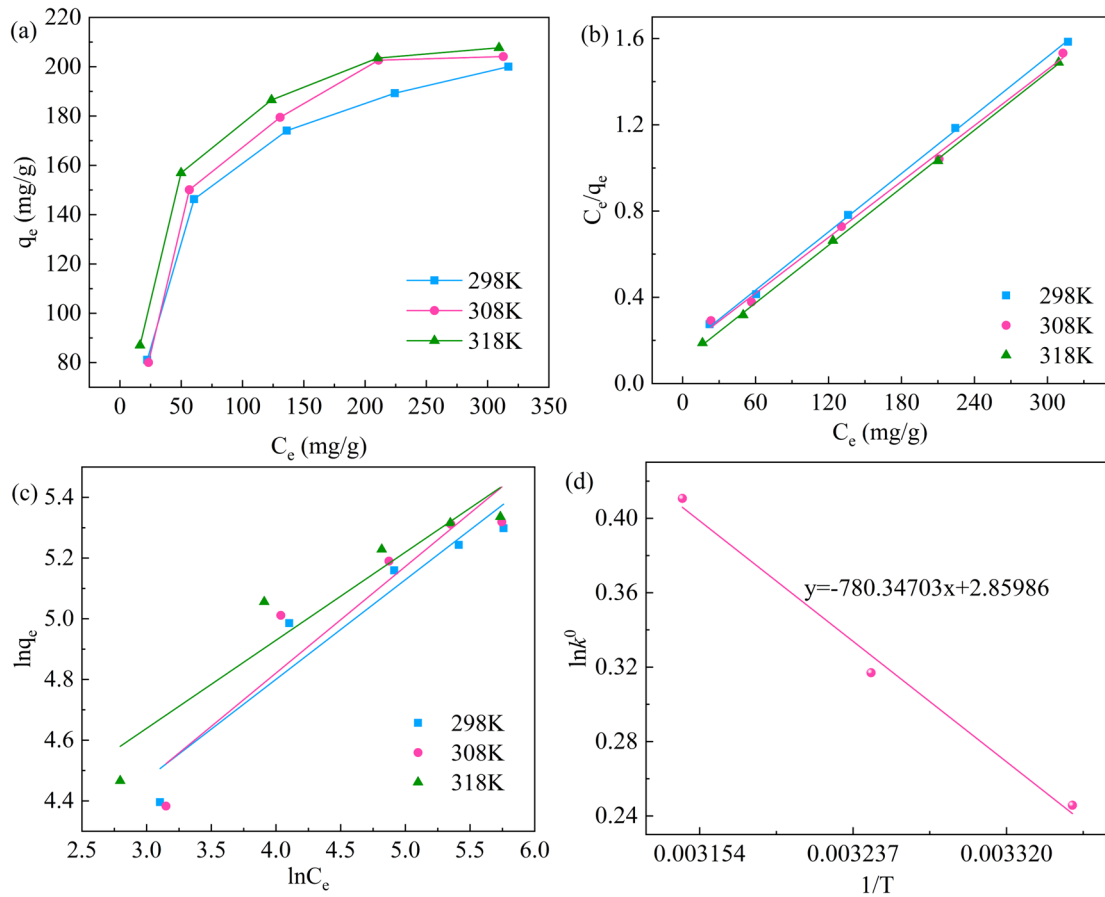


Fig. 6 a Effect of temperature on the adsorption capacity of SCB-A for Mo(VI) (pH=2, $t=3$ h); b Langmuir model; c Freundlich model

Table 3 Isotherm parameters of Mo(VI) adsorption on the SCB-A

	T(K)	Langmuir			Freundlich			
		q_{exp} (mg/g)	q_m (mg/g)	K_L (L/mg)	R^2	K_f	n	R^2
SCB-A	298	200.01	221.73	0.03	0.999	32.73	3.05	0.916
	308	204.14	231.48	0.03	0.997	30.46	2.85	0.887
	318	207.70	224.72	0.04	0.999	43.31	3.45	0.905

Table 4 Thermodynamics parameters of Mo(VI) adsorption on the SCB-A

C^0 (mg/l)	T (K)	k^0	$\ln k^0$	ΔG^0 (kJ/mol)	ΔH^0 (kJ/mol)	ΔS^0 (J/mol·K)
300	298	1.28	0.25	- 0.61	6.49	23.78
300	308	1.37	0.32	- 0.81		
300	318	1.51	0.41	- 1.09		

initial concentration of 500 mg/L at temperatures from 298 to 318 K. Virtually, the thermodynamics parameters can be acquired from the coefficient of thermodynamic distribution (K^0), i.e., equilibrium constant of the adsorption process [8]. According to the Van't Hoff equation (Eq. 11), the values of ΔH and ΔS can be calculated from the slope and intercept

of the thermodynamic graph of $\ln k^0$ versus $1/T$, as shown in Fig. 6d.

$$k^0 = \frac{C_0 - C_e}{C_e} \times \frac{V}{m}, \tag{9}$$

$$\Delta G^0 = -RT \ln k^0, \quad (10)$$

$$\ln k^0 = \frac{\Delta S^0}{R} - \frac{\Delta H^0}{RT}, \quad (11)$$

where C_0 is the initial concentration of the adsorbate in solution (mg/L); C_e is the equilibrium concentration of the adsorbate in solution (mg/L); k^0 is the distribution coefficient at each temperature (mL/g); V is the volume of solution (mL); m is the adsorbent weight (mg); ΔG^0 is the standard Gibbs free energy change (kJ/mol); R is the universal gas constant, (8.314 J/mol·K); T is the adsorption absolute temperature (K).

As shown in Table 4, the adsorption capacity raised from 200.01 mg/g to 207.70 mg/g when the temperature increased from 298 to 318 K, indicating molybdenum(VI) adsorption as an endothermic process. The negative ΔG^0 indicates that molybdenum(VI) adsorption on SCB-A was spontaneous in the research range. The positive ΔS^0 can be explained through the increase in randomness during the adsorption process, which can be related to the release of hydrogen ions or orderly structured hydration water. Also, the positive ΔH^0 demonstrates the endothermicity of molybdenum(VI) adsorption by SCB-A again. Therefore, the positive enthalpy (ΔH^0) change and the entropy (ΔS^0) increase collectively contribute to the strong spontaneous molybdenum(VI) adsorption by SCB-A [14].

Competitive Adsorption

The selective effect for target metal ions is a crucial factor in assessing the performance of the adsorbent. To evaluate

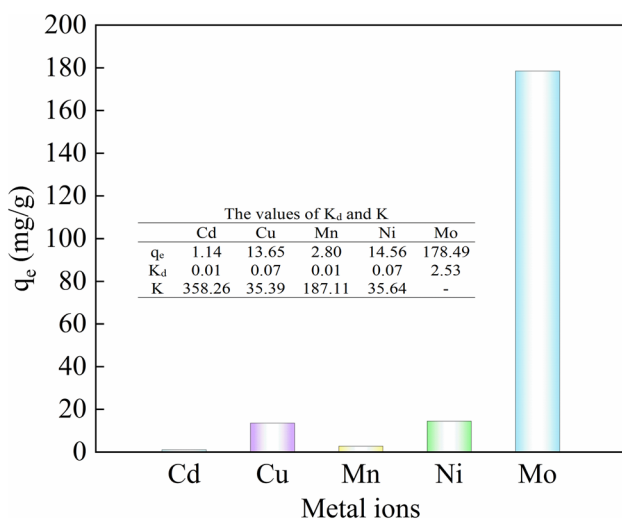


Fig. 7 Effect of coexisting metal ions on Mo(VI) adsorption (pH=2, $[Cd]_0 = [Cu]_0 = [Mn]_0 = [Ni]_0 = [Mo]_0 = 200$ mg/L, $t = 3$ h, $T = 25$ °C)

the selective performance of SCB-A, a multi-ion coexistence solution (Cd, Cu, Mn, Ni, and Mo) was used in the competitive experiment. As shown in Fig. 7, the adsorption capacity of SCB-A is about 178 mg/g on Mo, and both below 15 mg/g for other metal ions. In addition, the distribution coefficient (K_d) of SCB-A for Mo exceeded other metal ions evidently, indicating the excellent adsorption selectivity of SCB-A on Mo adsorption at pH 2.0. Therefore, SCB-A displays the ability of highly selective recognition of molybdenum from aqueous solution.

Regeneration Experiment

The regeneration ability is a significant factor in evaluating the suitability for actual applications of adsorbent [13]. The desorption effect for Mo(VI) in different eluents was investigated, as shown in Fig. 8a. The results show that both 10 mL 0.1 mol/L NaOH or EDTA exhibited higher desorption capacities for Mo(VI) in 20 min, but lower desorption capacities for Mo(VI) with HNO_3 as eluent under the same condition. This indicates that electrostatic absorption plays a primary part in SCB-A for Mo(VI) adsorption and 0.1 mol/L NaOH as eluent is used in the follow-up

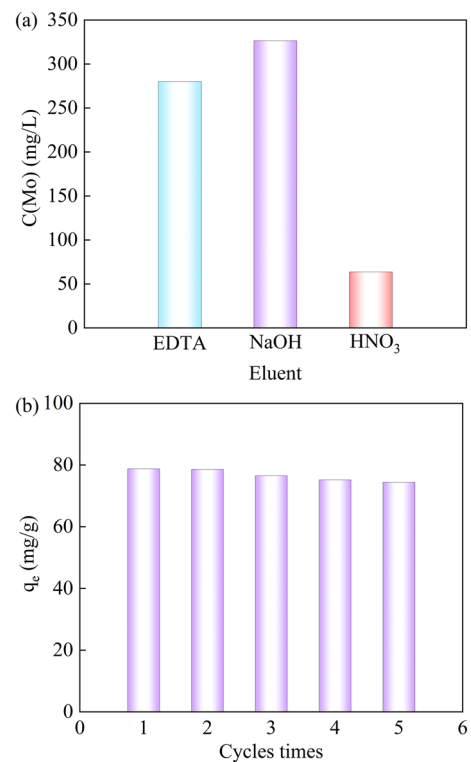


Fig. 8 a The desorption of Mo(VI) in different eluents (Desorption: Eluent as 0.1 mol/L 10 mL NaOH, EDTA and HNO_3 , $t = 20$ min); **b** The adsorption reusability of SCB-A for Mo(VI) (Desorption: Eluent as 0.1 mol/L 50 mL NaOH); (Adsorption: pH=2, $[Mo]_0 = 100$ mg/L, $t = 3$ h, $T = 25$ °C)

desorption experiments. As shown in Fig. 8b, the adsorption capacity of SCB-A adsorbent decreased slightly after the five cycles of absorption–desorption. Results show that SCB-A has excellent performance in adsorption stability and recycling and has economic potential in the water treatment process.

Possible Adsorption Mechanisms

Fourier Transform Infrared Spectroscopy Analysis

To explore the adsorption behavior of Mo(VI) on the amine-functionalized sugarcane bagasse (SCB-A), the differences of SCB, SCB-A, and SCB-A-M in FTIR spectra are shown in Fig. 9. In the FTIR spectrum, the peaks appearing at 3415.9 cm^{-1} and 3236.6 cm^{-1} and 2939.5 cm^{-1} correspond to the -O-H and -N-H and -C-H bonds, respectively [12, 29, 30]. After the amination of SCB with polyethylene polyamine, the peak of -N-H bonds at 3236.6 cm^{-1} in SCB-A is shifted to 3238.4 cm^{-1} in SCB-A-Mo(VI), and this blue shift where the stretching frequency increases and the bond length decreases was observed, which is probably attributed to the successful adsorption of Mo(VI) onto SCB-A [31, 32]. The peak at 1250 cm^{-1} in SCB is assigned to the C–O stretching vibration of secondary alcohol from cellulose and hemicellulose or guaiacyl unit from lignin, and this peak at 1250 cm^{-1} disappears in SCB-A, indicating the functionalization of amine on SCB [29]. The peak at 1720.5 cm^{-1} disappeared in SCB-A, which is probably due to the replacement of the acetyl group in hemicellulose with amine [29, 33]. All these changes give evidence of successful functionalization of the amine group on the bagasse surface. Compared with the spectra of the SCB-A to the SCB-A-M, the new band at 947 cm^{-1} in the spectrum of

SCB-A-Mo(VI) is due to the Mo=O [34], demonstrating the successful absorption for Mo(VI) onto amine-functionalized sugarcane bagasse (SCB-A).

X-ray Photoemission Spectroscopy (XPS)

To investigate the composition and distribution of elements in SCB-A before and after adsorption, the XPS analysis was carried out, as displayed in Fig. 10 and Table 5. In the full-scan spectrum of the SCB-A before adsorption, three principal peaks corresponding to C 1 s, N 1 s, and O 1 s are observed in Fig. 10a. The typical peaks of Mo 3d appeared in the SCB-A spectrum after adsorption, indicating that Mo(VI) in aqueous solution was successfully absorbed by the SCB-A.

The Mo 3d spectra displayed that the two doublets can be divided, wherein one doublet with Mo $3d_{5/2}$ (232.94 eV) and Mo $3d_{3/2}$ (236.04 eV) peaks is ascribed to Mo–O bond of MoO_3 (Mo(VI)), respectively, and the other doublet with Mo $3d_{5/2}$ (231.79 eV) and Mo $3d_{3/2}$ (234.75 eV) peaks is ascribed to Mo–O bond of MoO_2 (Mo(IV)), respectively [35, 36]. The coexistence of both Mo(VI) and Mo(IV) reveals that a part of Mo(VI) has been transformed into Mo(IV) during the adsorption reaction [37]. This was possibly related to the redox reaction in the adsorption process. The C1s spectrum reveals that the peaks of C–C, C–N, and C=O, shifted from 284.81 eV , 286.47 eV , and 287.99 to 284.88 eV , 286.51 eV , and 287.97 eV after adsorption, respectively [29, 38]. The O1s spectra show three peaks located at 531.29 eV , 532.18 eV , and 534.31 eV , corresponding to C=O, C–O, and O–H, respectively, shifted to 530.94 eV , 532.97 eV , and 534.20 eV after adsorption [38, 39]. The possible explanation for this phenomenon is the adsorption function

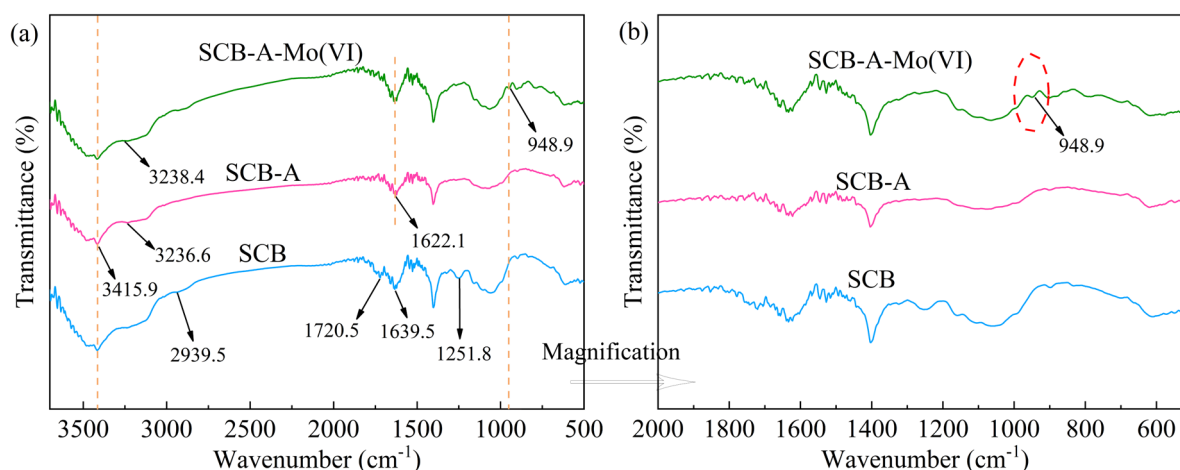


Fig. 9 FTIR spectra of the sugarcane bagasse (SCB), amine-functionalized sugarcane bagasse before (SCB-A) and after adsorption (SCB-A-Mo(VI))

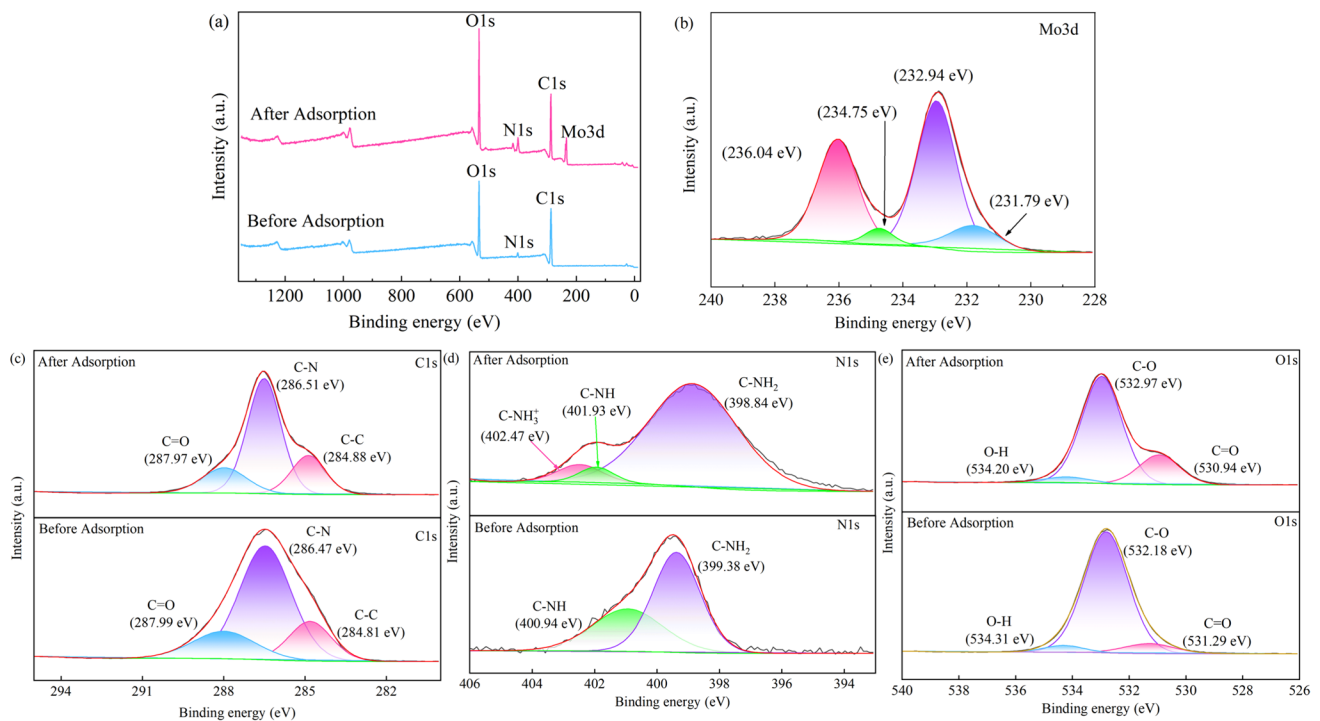


Fig. 10 XPS full-scan spectrum (a) and high-resolution spectra of Mo 3d (b), C 1 s (c), N 1 s (d), and O1s (e) of SCB-A before and after adsorption

Table 5 Binding energies and composition for SCB-A before and after adsorption

Band	Bond	Before adsorption	After adsorption
Binding energy (eV)			
C 1 s	C–C	284.81	284.88
	C–N	286.47	286.51
	C=O	287.99	287.97
O 1 s	C=O	531.29	530.94
	C–O	532.18	532.97
	O–H	534.31	534.20
N 1 s	C–NH ₂	399.38	398.84
	C–NH	400.94	401.93
	C–NH + 3	–	402.47
Mo 3d	MoO ₃	–	232.94, 236.04
	MoO ₂	–	231.79, 234.75
Atomic surface composition (%)			
C 1 s		64.68	52.23
O 1 s		31.91	36.33
N 1 s		3.40	9.16
Mo 3d		–	2.28

of O–H in SCB-A for Mo(VI). The N1s spectrum displays two peaks at 399.38 eV and 400.94 eV, corresponding to C–NH₂ and C–NH, respectively. After adsorption, the peaks of C–NH₂ and C–NH shifted to 398.84 eV and

401.93 eV, and a new peak of 402.47 eV was exhibited (Corresponding to C–NH + 3) [29, 38].

At pH 2.0, H₃Mo₇O₃^{–24} as the main species of molybdenum in aqueous solution [21] can interact with –NH + 3 on the surface of SCB-A electrostatically, which leads to the deposition of the negatively charged H₃Mo₇O₃^{–24} on the positively charged surface of SCB-A. Mo(VI) is subsequently reduced to Mo(IV) by –NH + 3, thereby exhibiting the coexistence of both Mo(VI) and Mo(IV). Results demonstrate that Mo(VI) was successfully adsorbed with protonated amine groups on SCB-A by electrostatic interaction. In conclusion, the possible mechanism for the adsorption of Mo(VI) with SCB-A is shown in Fig. 11.

Conclusions

In this work, the amine-functionalized sugarcane bagasse adsorbent (SCB-A) has been synthesized by the sugarcane bagasse with polyethylene polyamine-grafted, and its adsorption behavior on Mo(VI) was explored. The SEM–EDS, BET, TG, FITR, and XPS analysis indicated the successful grafting of polyethylene polyamine onto sugarcane bagasse and its successful adsorption for Mo(VI). Besides, the thermogravimetry analysis confirmed the good thermal stability of SCB-A. 1 g/L of the adsorbent dosage at pH 2.0 was selected for further experiments by synthetically

Fig. 11 Possible adsorption mechanism of Mo(VI) with SCB-A



considered. Adsorption isotherms and kinetics show that this adsorption reaction is a spontaneous endothermic process, and its theoretical maximum adsorption capacity is about 231.48 mg/g. The adsorption capacity was 8.93-fold compared to that of pristine sugarcane bagasse. This adsorption process was more consistent with the Langmuir model and pseudo-second-order kinetics model, indicating that this process was monolayer adsorption on a homogeneous surface and the adsorption rate was controlled by the chemisorption process. SCB-A exhibits high adsorption capacity and great selective recognition properties toward Mo(VI) in a multi-ion coexistence solution. Moreover, SCB-A possesses excellent performance in adsorption stability and recycling, and it has tremendous potential in the economically and feasible removal of Mo(VI) from wastewater.

Acknowledgements This work was supported by the Hunan Provincial Natural Science Foundation of China (No. 2020JJ5456), the Hunan Provincial Innovation Foundation for Postgraduate (No. CX20221108), and the Innovation and Entrepreneurship Training Program for College Students (JDCX2021459).

Declarations

Conflict of interest On behalf of all authors, the corresponding author states that there is no conflict of interest.

References

- Wu L, Luo Z, Jiang H, Zhao Z, Geng W (2021) Selective and rapid removal of Mo(VI) from water using functionalized Fe₃O₄-based Mo(VI) ion-imprinted polymer. *Water Sci Technol* 83(2):435–448. <https://doi.org/10.2166/wst.2020.594>
- Rout PC, Mishra GK, Padh B, Suresh KR, Ramachandra Reddy B (2017) Solvent extraction separation of molybdenum as thio-molybdate complex from alkaline tungsten leach liquor of spent HDS catalyst—a pilot study. *Hydrometallurgy* 174:140–146. <https://doi.org/10.1016/j.hydromet.2017.10.002>
- Ren Y, Liu P, Feng J, Ma J, Wen Q, Zhang M (2013) Selective recognition of molybdenum(VI) from water by Mo(VI) oxyion-imprinted particle as an adsorbent. *Chem Eng J* 219:286–294. <https://doi.org/10.1016/j.cej.2013.01.018>
- Arda C, Frau F, Dore E, Lattanzi P (2012) Molybdate sorption by Zn–Al sulphate layered double hydroxides. *Appl Clay Sci* 65–66:128–133. <https://doi.org/10.1016/j.clay.2012.05.005>
- Wu X, Zhang G, Zeng L, Zhou Q, Li Z, Zhang D, Cao Z, Guan W, Li Q, Xiao L (2019) Study on removal of molybdenum from ammonium tungstate solutions using solvent extraction with quaternary ammonium salt extractant. *Hydrometallurgy* 186:218–225. <https://doi.org/10.1016/j.hydromet.2019.04.006>
- Nguyen TH, Lee MS (2013) Separation of molybdenum and vanadium from acid solutions by ion exchange. *Hydrometallurgy* 136:65–70. <https://doi.org/10.1016/j.hydromet.2013.03.007>
- Djedidi Z, Bouda M, Souissi MA, Cheikh RB, Mercier G, Tyagi RD, Blais J-F (2009) Metals removal from soil, fly ash and sewage sludge leachates by precipitation and dewatering properties of the generated sludge. *J Hazard Mater* 172(2–3):1372–1382. <https://doi.org/10.1016/j.jhazmat.2009.07.144>
- Fallah N, Taghizadeh M, Hassanpour S (2018) Selective adsorption of Mo(VI) ions from aqueous solution using a surface-grafted Mo(VI) ion imprinted polymer. *Polymer* 144:80–91. <https://doi.org/10.1016/j.polymer.2018.04.043>
- Martín-Lara MÁ, Rico ILR, Vicente IDLCA, García GB, de Hoces MC (2010) Modification of the sorptive characteristics of sugarcane bagasse for removing lead from aqueous solutions. *Desalination* 256(1–3):58–63. <https://doi.org/10.1016/j.desal.2010.02.015>
- Yu J, Xiong W, Zhu J, Chen J, Chi R (2016) Removal of Congo red from aqueous solution by adsorption onto different amine compounds modified sugarcane bagasse. *Clean Technol Environ Policy* 19(2):517–525. <https://doi.org/10.1007/s10098-016-1243-7>
- Irawan C, Putra MD, Wijayanti H, Juwita R, Meliana Y, Nata IF (2021) The amine functionalized sugarcane bagasse biocomposites as magnetically adsorbent for contaminants removal in aqueous solution. *Molecules* 26(19):5867. <https://doi.org/10.3390/molecules26195867>
- Abdelwahab NA, Shukry N, El-kalyoubi SF (2020) Separation of emulsified oil from wastewater using polystyrene and surfactant modified sugarcane bagasse wastes blend. *Clean Technol Environ Policy* 23(1):235–249. <https://doi.org/10.1007/s10098-020-01973-1>
- Zong E, Guo B, Yang J, Shi C, Jiang S, Ma Z, Liu X (2020) Reusable hyperbranched polyethylenimine-functionalized ethyl cellulose film for the removal of phosphate with easy separation. *ACS Omega* 6(1):505–515. <https://doi.org/10.1021/acsomega.0c04955>
- Xiang H, Yang Z, Min X, Liang Y, Peng C, Liu X, Yuan R, Wang Q, Zhao F (2023) Enhanced recovery of germanium(IV) from zinc residue leachate by tartaric acid functionalized chitosan: experiments and DFT calculation. *Hydrometallurgy* 221:106121. <https://doi.org/10.1016/j.hydromet.2023.106121>

15. Chen L, Wu K, Zhang M, Liu N, Li C, Qin J, Zhao Q, Ye Z (2023) Synthesis of carbon disulfide modified chitosan resin and its adsorption properties for palladium(II) in wastewater. *Chem Eng J* 466:143082. <https://doi.org/10.1016/j.cej.2023.143082>
16. Huang Z, Huang Z, Feng L, Luo X, Wu P, Cui L, Mao X (2018) Modified cellulose by polyethyleneimine and ethylenediamine with induced Cu(II) and Pb(II) adsorption potentialities. *Carbohydr Polym* 202:470–478. <https://doi.org/10.1016/j.carbpol.2018.08.136>
17. Wang Y, Dang Q, Liu C, Yu D, Pu X, Wang Q, Gao H, Zhang B, Cha D (2018) Selective adsorption toward Hg(II) and inhibitory effect on bacterial growth occurring on thiosemicarbazide-functionalized chitosan microsphere surface. *ACS Appl Mater Interfaces* 10(46):40302–40316. <https://doi.org/10.1021/acsami.8b14893>
18. Peng X, Wu Z, Li Z (2020) A bowl-shaped biosorbent derived from sugarcane bagasse lignin for cadmium ion adsorption. *Cellulose* 27(15):8757–8768. <https://doi.org/10.1007/s10570-020-03376-3>
19. Zhang L, Xue J, Zhou X, Fei X, Wang Y, Zhou Y, Zhong L, Han X (2014) Adsorption of molybdate on molybdate-imprinted chitosan/triethanolamine gel beads. *Carbohydr Polym* 114:514–520. <https://doi.org/10.1016/j.carbpol.2014.08.049>
20. Gao X, Cao Z, Li C, Liu J, Liu X, Guo L (2022) Activated carbon fiber modified with hyperbranched polyethylenimine and phytic acid for the effective adsorption and separation of In(III). *New J Chem* 46(39):18952–18960. <https://doi.org/10.1039/d2nj03111f>
21. Li F, Peng M, Hu Z, Liu C, Xiao L, Liu Z, Yan W (2023) Research progress in separation of molybdenum(VI) and iron(III) in acidic solutions by solvent extraction. *Min Metall Eng* 43(02):118–124
22. Wang Q, Zhu S, Xi C, Shen Y, Xiang Y, Zhang F (2021) The cross-linked hyperbranched polyamide-amines: the preparation and its adsorption for Pb(II). *J Appl Polym Sci* 139(13):51866. <https://doi.org/10.1002/app.51866>
23. Gao L, Wang L, Cao Y, Li S (2022) Persimmon peel-based ion-imprinted adsorbent with enhanced adsorption performance of gallium ions. *Miner Eng* 176:107354. <https://doi.org/10.1016/j.mineng.2021.107354>
24. Li W, Dong X, Zhu L, Tang H (2020) Highly selective separation of Re(VII) from Mo(VI) by using biomaterial-based ionic gel adsorbents: extractive adsorption enrichment of Re and surface blocking of Mo. *Chem Eng J* 387:124078. <https://doi.org/10.1016/j.cej.2020.124078>
25. Wang Y, Yang K, Wang J, Yu H, Cui J, Xiong Y (2021) Preparation of porous Mo(VI)-imprinted algae for recognizing molybdenum(VI). *Solv Extr Ion Exch* 39(5–6):622–638. <https://doi.org/10.1080/07366299.2021.1876985>
26. Su S, Liu Q, Liu J, Zhang H, Li R, Jing X, Wang J (2018) Functionalized sugarcane bagasse for U(VI) adsorption from acid and alkaline conditions. *Sci Rep* 8(1):793. <https://doi.org/10.1038/s41598-017-18698-9>
27. Machado TS, Crestani L, Marchezi G, Melara F, de Mello JR, Dotto GL, Piccin JS (2022) Synthesis of glutaraldehyde-modified silica/chitosan composites for the removal of water-soluble diclofenac sodium. *Carbohydr Polym* 277:118868. <https://doi.org/10.1016/j.carbpol.2021.118868>
28. Zeng Q, Wang S, Hu L, Zhong H, He Z, Sun W, Xiong D (2021) Oxalic acid modified copper tailings as an efficient adsorbent with super high capacities for the removal of Pb²⁺. *Chemosphere* 263:127833. <https://doi.org/10.1016/j.chemosphere.2020.127833>
29. Ravi K, Gbe J-LK, Mehra S, Tothadi S, Kumar A, Biradar AV (2023) Functional bagasse: as a versatile catalyst for Henry reaction and additive-free cycloaddition of CO₂. *J Environ Chem Eng* 11(3):109737. <https://doi.org/10.1016/j.jece.2023.109737>
30. Abdelwahab NA, Shukry N (2015) Synthesis, characterization and antimicrobial properties of grafted sugarcane bagasse/silver nanocomposites. *Carbohydr Polym* 115:276–284. <https://doi.org/10.1016/j.carbpol.2014.08.052>
31. Behera B, Das PK (2018) Blue and red shifting hydrogen bonding: a gas phase FTIR and Ab initio study of RR'CO-DCCl₃ and RR'S-DCCl₃ complexes. *J Phys Chem A* 122(18):4481–4489. <https://doi.org/10.1021/acs.jpca.7b11962>
32. Kannan PP, Karthick NK, Mahendraprabu A, Shanmugam R, Elangovan A, Arivazhagan G (2017) Red/blue shifting hydrogen bonds in acetonitrile—dimethyl sulphoxide solutions: FTIR and theoretical studies. *J Mol Struct* 1139:196–201. <https://doi.org/10.1016/j.molstruc.2017.03.036>
33. Li R, Fei J, Cai Y, Li Y, Feng J, Yao J (2009) Cellulose whiskers extracted from mulberry: a novel biomass production. *Carbohydr Polym* 76(1):94–99. <https://doi.org/10.1016/j.carbpol.2008.09.034>
34. Xiao C, Zeng L, Xiao L, Zhang G (2017) Solvent extraction of molybdenum (VI) from hydrochloric acid leach solutions using P507. Part I: extraction and mechanism. *Solv Extr Ion Exch* 35(2):130–144. <https://doi.org/10.1080/07366299.2017.1308154>
35. Liu R, Zhao Z, Li Y (2023) Acid leaching–extraction–circulation process based on Mo(VI) coordination with H₃PO₄ to efficiently extract molybdenum from different components of molybdenum calcine. *Sep Purif Technol* 322:124269. <https://doi.org/10.1016/j.seppur.2023.124269>
36. El Din AMS, Sayed MA, Monir TM, Sami NM, Aly AMI (2021) Sponge-like Ca-alginate/Lix-84 beads for selective separation of Mo(VI) from some rare earth elements. *Int J Biol Macromol* 184:689–700. <https://doi.org/10.1016/j.jbiomac.2021.06.138>
37. Bai L, Su X, Feng J, Ma S (2021) Preparation of sugarcane bagasse biochar/nano-iron oxide composite and mechanism of its Cr (VI) adsorption in water. *J Clean Prod* 320:128723. <https://doi.org/10.1016/j.jclepro.2021.128723>
38. Gómez-Navarro CS, Warren-Vega WM, Serna-Carrizales JC, Zárate-Guzmán AI, Ocampo-Pérez R, Carrasco-Marín F, Collins-Martínez VH, Niembro-García J, Romero-Cano LA (2022) Evaluation of the environmental performance of adsorbent materials prepared from agave bagasse for water remediation: solid waste management proposal of the tequila industry. *Materials* 16(8):1–17. <https://doi.org/10.3390/ma16010008>
39. Elias MMC, Soares LC, Maia LC, Taylor JG, Adarme OFH, Ferreira GMD, de Azevedo ER, de Siervo A, da Silva LHM, Gurgel LVA (2023) Batch and continuous adsorption of Cd(II) and Pb(II) on polycarboxylated sugarcane bagasse. *J Water Process Eng* 54:103947. <https://doi.org/10.1016/j.jwpe.2023.103947>

Publisher's Note Springer Nature remains neutral with regard to jurisdictional claims in published maps and institutional affiliations.

Springer Nature or its licensor (e.g. a society or other partner) holds exclusive rights to this article under a publishing agreement with the author(s) or other rightsholder(s); author self-archiving of the accepted manuscript version of this article is solely governed by the terms of such publishing agreement and applicable law.